ICAS-84-1.3.3

NUMERICAL SOLUTIONS OF THE EULER EQUATIONS GOVERNING AXISYMMETRIC AND THREE-DIMENSIONAL TRANSONIC FLOW

D.M. Causon and P.J. Ford
Department of Aeronautical and Mechanical Engineering
University of Salford
Salford M5 4WT
U.K.

Abstract

A computational method is presented for solving numerically the three dimensional Euler equations for transonic flow around practical aircraft forebodies. The Euler solver is pseudo-time dependent, split and cast in finite volume form. Shock waves are captured crisply without the need for additional smoothing by means of an operator-switching facility which more accurately reflects the direction of propagation of signals.

The method is illustrated by examples of computed external, axisymmetric flows and some, simulated, realistic aircraft forebodies. The computational meshes employed in the three dimensional cases are essentially of cylindrical polar, flow conforming, type and relatively coarse. Closer attention to the mesh generation is expected to refine the results presented here. The method is versatile, robust, and holds promise for treating complex three dimensional geometries within economically viable run times.

Introduction

Computational aerodynamics has become a powerful tool in the armoury of aerodynamicists. The last fifteen years has seen a rapid advancement in computer technology, paced by an almost equally rapid improvement in numerical algorithms applied to fluid flows. The early transonic flow solvers of Magnus and Yoshihara[1] and Murman and Cole[2] have been the basis for successively more refined algorithms, particularly those based on the full potential equation and currently used in many design offices. Recently, these codes have been applied, using the multi-block approach, to near complete aircraft configurations, including engines and stores. A particular feature is the solving of the flow field-equations in physical space on Cartesian grids, thus circumventing the difficult problem of mesh generation. The work of Rehyner[3] and Boppe[4] exemplify this approach. Full-potential codes have the advantage that they are economical to run and, when combined with an appropriate optimisation code, can be put to work to sort through a range of possible designs, or to explain how configuration changes will affect the features of the flowfield.

However, whilst potential methods have demonstrated a capability for predicting transonic flows with shocks of moderate strength, the approximations made in ignoring entropy changes and vorticity production cannot reasonably be expected to yield acceptable accuracy when the flight Mach number is in the low supersonic range typically encountered in design studies of proposed fighter aircraft. Also, there is some evidence[5] of non-unique solutions arising from solving the full-potential equation. Accordingly, one is led to the conclusions that we must solve the more exact Euler equations to provide an accurate description of the inviscid transonic flow past realistic configurations.

Although Euler solvers should, in principle, furnish more accurate predictions of the features of inviscid flows, they are not without deficiencies. Probably the most serious problem areas are those which relate respectively to the accurate resolution of captured shock profiles, without oscillations, and the minimising of spurious entropy production. These negative features have been the stimulus for much recent algorithm research and development. There have been those workers[6-9] who have concentrated their efforts on the development and refinement of existing methods, and those who have researched new ones. In the latter category are the impressive flux-splitting methods of Roe[10,11], Osher[12] and others[13,14] which have successfully been applied to very strong shock waves and blast waves. Methods in the former category have, in contrast, tended to be applied to aeronautical fluid flows where shock waves are not as severe, but, perhaps, geometrically more complex. This tends to suggest that one should view the available methods in a heirarchal light, with the computationally inexpensive full potential methods at a lower level than the very expensive but high-precision flux-difference splitting methods. One would then choose the most appropriate algorithm for the problem to be solved.

Our approach is based upon algorithm development, and so lies somewhere in the middle of the above heirarchy. It uses the finite volume concept, split operators and a switching process which implements the spatially-symmetric, explicit, MacCormack method in subsonic regions of the flowfield and switches to a scheme incorporating spatial bias in supersonic regions. Captured shock profiles are crisp and well defined. The method does not drop to first-order accuracy in the vicinity of shock waves, as do other methods, nor does it require substantial doses of added smoothing.

In the following sections of this paper the differential and integral formulations of the equations of motion are reviewed, the numerical discretisation procedure is outlined and a range of computed results are presented, relating to axisymmetric external flows and some realistic aircraft forebodies. The axisymmetric flow results serve to illustrate a direct comparison between the MacCormack split algorithm and the operator-switching approach. We conclude with some remarks on mesh generation with reference to likely future applications of our method.

Differential and Integral Formulation

The finite volume method uses a general system of non-orthogonal co-ordinates which conform to the body contour. The curvilinear system with contravariant co-ordinates x^ℓ and covariant base vectors $\underline{g}_\ell$ is introduced, the intersections of the respective co-ordinate surfaces constituting a network of mesh cells. Intrinsically related are the contravariant field vectors $\underline{g}^m = \text{grad } x^m$ and related to the base vectors by $\underline{g}^m.\underline{g}_\ell = \delta^m_\ell$. Between these co-ordinates and a rectangular Cartesian system Z_m, with unit based vectors $\underline{a}_m$, there exists the functional relationship.

$$x^\ell = x^\ell\,(Z_1,Z_2,Z_3),\ \ell = 1,2,3. \tag{1}$$

The Euler equations when written in strong conservation form with respect to this curvilinear system are

$$\frac{\partial}{\partial t}(\sqrt{g}\underline{U}) + \frac{\partial}{\partial x^\ell}(\sqrt{g}\,\underline{\underline{F}}^\ell) = 0 \tag{2}$$

or

$$(\sqrt{g}\underline{U})_{,t} + (\sqrt{g}\,\underline{\underline{F}}^\ell)_{,\ell} = 0$$

where

$$\underline{U} = [\rho, \rho w_1, \rho w_2, \rho w_3, e]^T,$$

$$\underline{\underline{F}}^\ell(U) = \begin{bmatrix} \rho u^\ell \\ \rho w_1 u^\ell + p\frac{\partial x^\ell}{\partial Z_1} \\ \rho w_2 u^\ell + p\frac{\partial x^\ell}{\partial Z_2} \\ \rho w_3 u^\ell + p\frac{\partial x^\ell}{\partial Z_3} \\ (e+p)u^\ell \end{bmatrix},\ \ell = 1,2,3$$

the Jacobian $\sqrt{g} \equiv \partial(Z_1,Z_2,Z_3)/\partial(x^1,x^2,x^3)$ and we note for later convenience that the flow velocity can be written as $\underline{q} = u^\ell \underline{g}_\ell = w_\ell \underline{a}_\ell$, where $\underline{a}_\ell$ are the unit Cartesian base vectors.

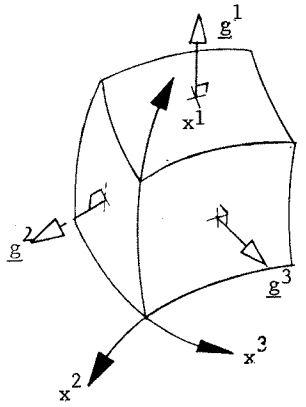

FIG. 1

Formation of finite volume cell by intersections of surfaces x^ℓ = const.

Equation (2) can be rewritten in the form

$$(\sqrt{g}\underline{U})_{,t} + \nabla.\tau = 0 \tag{3}$$

where $\nabla.\tau = \nabla(\underline{\underline{F}}^1\underline{g}_1 + \underline{\underline{F}}^2\underline{g}_2 + \underline{\underline{F}}^3\underline{g}_3)$. Then by applying Gauss' theorem (3) may be cast in integral form

$$(\sqrt{g}\underline{U})_{,t} + \iint_{S1}\underline{\underline{F}}^1\,ds + \iint_{S2}\underline{\underline{F}}^2\,ds + \iint_{S3}\underline{\underline{F}}^3\,ds = 0 \tag{4}$$

which emphasises the amenability of the equations to splitting with respect to the co-ordinate directions x^ℓ with which S^ℓ are associated.

Now, since $\frac{\partial x^\ell}{\partial Z_m} = \underline{g}^\ell.\underline{a}_m$ and $\underline{q}.\underline{g}^\ell = u^\ell$

we have

$$\underline{\underline{F}}^\ell(U) = \begin{bmatrix} \rho\underline{q}.\underline{g}^\ell \\ \rho w_1\underline{q}.\underline{g}^\ell + p\underline{g}^\ell.\underline{a}_1 \\ \rho w_2\underline{q}.\underline{g}^\ell + p\underline{g}^\ell.\underline{a}_2 \\ \rho w_3\underline{q}.\underline{g}^\ell + p\underline{g}^\ell.\underline{a}_3 \\ (e+p)\underline{q}.\underline{g}^\ell \end{bmatrix} = \begin{bmatrix} \rho\underline{q} \\ \rho w_1\underline{q} + p\underline{a}_1 \\ \rho w_2\underline{q} + p\underline{a}_2 \\ \rho w_3\underline{q} + p\underline{a}_3 \\ (e+p)\underline{q} \end{bmatrix} .\underline{g}^\ell$$

Then

$$\sqrt{g}\,\underline{\underline{F}}^\ell(\underline{U}) = \begin{bmatrix} \rho\underline{q} \\ \rho w_1\underline{q} + p\underline{a}_1 \\ \rho w_2\underline{q} + p\underline{a}_2 \\ \rho w_3\underline{q} + p\underline{a}_3 \\ (e+p)\underline{q} \end{bmatrix} .\sqrt{g}\,\underline{g}^\ell.$$

$$= \underline{\underline{H}}(\underline{U}).\underline{S}^\ell \tag{5}$$

where $\sqrt{g}$ is the volume of the computational cell and the term $\sqrt{g}\,\underline{g}^\ell$ is the contravariant, outward-pointing, surface normal for the surface x^ℓ = constant, hereafter denoted by $\underline{S}^\ell$.

Thus, finite volume computations can be performed with the more easily constructed flux tensor $\underline{\underline{H}}(\underline{U})$, comprising variables referenced only to the Cartesian frame. The area vector $\underline{S}^\ell$ 'splits' the tensor appropriately into components associated with each curvilinear direction. The evaluation of the area vectors and the volumes of the computational cells is easily accomplished using simple vector relations[15,16].

Numerical Procedure

The integral equations (4) are solved using a factored sequence of locally one-dimensional operators in the manner described by Strang[17].

Split Operators

Equation (2) can be split into three LOD differential operators as

$$L_\ell\ \sqrt{g}\,\underline{U}_{,t} + \underline{\underline{F}}^\ell{}_{,\ell} = 0 \text{ (no summation in } \ell) \tag{6}$$

where each split operator contains curvilinear spatial flux derivatives in one co-ordinate direction only. If we now let Δt be the time step, n the time level and $^{\ell}\underline{\underline{F}}$ be the flux across cell surface x^{ℓ} = constant, the MacCormack, fractional step, predictor-corrector difference operator $L_{\ell}(\Delta t)$ is

$$\underline{\text{predictor}} \quad \sqrt{g}\underline{U}^{n+1} = \sqrt{g}\underline{U}^{n} - \Delta t \left(\frac{\Delta_{-}\, {}^{\ell}\underline{\underline{F}}}{\Delta x^{\ell}}\right)^{n} \tag{7a}$$

$$\underline{\text{corrector}} \quad \sqrt{g}\underline{U}^{n+1} = \tfrac{1}{2}\left(\sqrt{g}\underline{U}^{n} + \sqrt{g}\underline{U}^{n+1} - \Delta t \left(\frac{\Delta_{+}\, {}^{\ell}\underline{\underline{F}}}{\Delta x^{\ell}}\right)^{n+1}\right) \tag{7b}$$

Here the overbars indicate predicted values and Δ_{+}, Δ_{-} are respectively forward and backward two point differences.

In finite volume form the operator $L_1(\Delta t)$ is then,

$$\underset{\sim}{U}^{n+1}_{ijk} = \underset{\sim}{U}^{n}_{ijk} - \Delta t \left(\underline{\underline{H}}^{n}_{ijk}\, \underline{S}_{i+\frac{1}{2}} + \underline{\underline{H}}^{n}_{i-1jk}\, \underline{S}_{i-\frac{1}{2}}\right) \tag{8a}$$

$$\underset{\sim}{U}^{n+1}_{jk} = \tfrac{1}{2}\left(\underset{\sim}{U}^{n}_{ijk} + \underset{\sim}{U}^{n+1}_{ijk} - \Delta t \left(\underline{\underline{H}}^{n+1}_{i+1jk}\, \underline{S}_{i+\frac{1}{2}} + \underline{\underline{H}}^{n+1}_{ijk}\, \underline{S}_{i-\frac{1}{2}}\right)\right) \tag{8b}$$

where $\underset{\sim}{U}_{ijk} = (\text{vol}\ \underline{U})_{ijk}$ evaluated at the cell centre ijk and $\underline{S}_{i\pm\frac{1}{2}}$ are the area vectors on opposite faces of the cell, corresponding to the co-ordinate surface x^1 = constant.

Scheme (7) is stable if[15]

$$\Delta t = \Delta t_{\ell} \leq \frac{\Delta x^{\ell}}{|u^{\ell}| + a} \tag{9}$$

where a is the speed of sound. For a given cell there will be three values of Δt_{ℓ}, one corresponding to each split, so we must choose either

$$\Delta t = \min\ (\Delta t_{\ell}),\quad \ell = 1,2,3 \tag{10}$$

if we are using local time stepping and are interested only in the steady state solution, or a global minimum time step

$$\Delta t = \min_{i,jk}\ (\Delta t_{\ell}),\quad = 1,2,3 \tag{11}$$

if time-accuracy is required.

Operator-Switching

The MacCormack operator (7) is spatially symmetric at the end of the corrector step and thus allows non-physical upstream propagation of data in regions where the flow is supersonic. This has a number of disadvantages.

1. A numerical boundary condition is required at a supersonic exit and this must carefully be implemented, since any erroneous data would propagate upstream into the flowfield and corrupt the solution.

2. Saw-tooth oscillations appear around captured shock waves, degrading accurate resolution of the profile.

3. Additional smoothing is required in the region of stagnation points, sonic lines and around shock waves.

These disadvantages do not apply to the MacCormack scheme alone but would apply equally to any second-order accurate and spatially-symmetric difference operator.

Various remedies have been proposed by researchers, ranging from the rigorous to the palliative. The flux-difference splitting and associated approaches[10-14] seek rigorously to match the spatial differencing to the direction of propagation of signals. They have been applied successfully in one and two-dimensions to capture very strong shock waves and blast waves, but they tend to be rather computationally expensive. Other approaches drop to a first-order scheme in the vicinity of shock waves[18], add a dose of artificial dissipation to attenuate oscillations[19], or employ a 'filter' to remove them[20].

There are two disadvantages associated with added smoothing. One is that the exact amount to be added will generally be unknown and may be subject to numerical experiments. The other is that, generally, spurious entropy production, arising particularly near stagnation points, is exacerbated by smoothing. Some of the negative features outlined above can be seen in Fig. 2, which depicts the numerical solution obtained by the MacCormack algorithm for a NACA 0012 aerofoil at M = 0.85 and $\alpha = 0^{o}$.

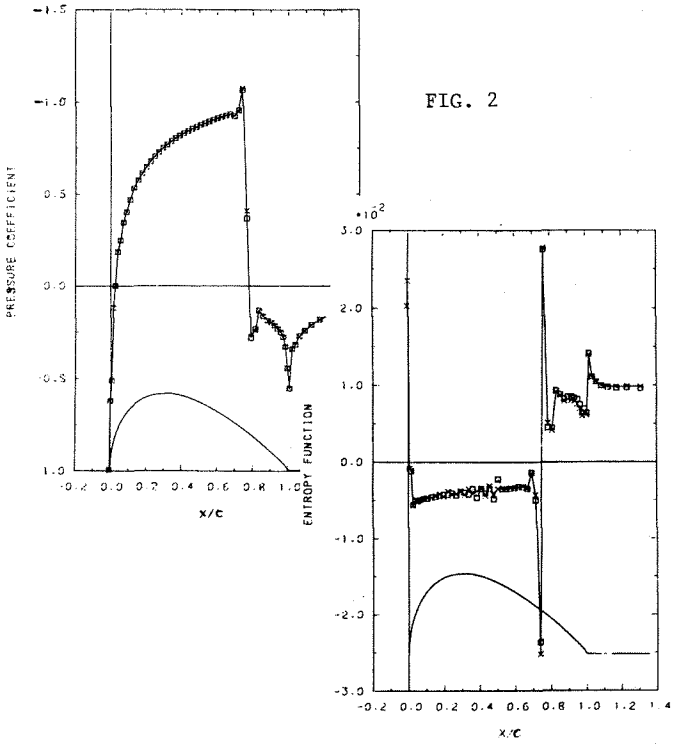

FIG. 2

Our approach involves switching, within any given split, between the MacCormack scheme and the upwind scheme of Beam and Warming[21]. The MacCormack scheme is employed wherever the flowfield is subsonic and the upwind scheme, which, as its name implies, incorporates spatial bias is implemented in supersonic regions. Both schemes are explicit and spatially second-order accurate. The upwind scheme, which is the counterpart of (7) is

$$\underline{\text{predictor}}\quad \sqrt{g}\overline{\underline{U}^{n+1}} = \sqrt{g}\underline{U}^{n} - \Delta t\ (\frac{\Delta - {}^{\ell}\underline{F}}{\Delta x^{\ell}})^{n} \qquad (12a)$$

$$\underline{\text{corrector}}\quad \sqrt{g}\underline{U}^{n+1} = \tfrac{1}{2}(\sqrt{g}\underline{U}^{n} + \sqrt{g}\overline{\underline{U}^{n+1}} - \Delta t(\frac{\Delta - {}^{\ell}\underline{\underline{F}}}{\Delta x^{\ell}})^{\overline{n+1}}$$

$$- \Delta t\ (\frac{\Delta^{2} - {}^{\ell}\underline{\underline{F}}}{\Delta x^{\ell}})^{n}). \qquad (12b)$$

When written in finite volume form, the upwind counterpart of the $L_1(\Delta t)$ operator (8) is

$$\overline{\underset{\sim}{U}^{n+1}_{ijk}} = \underset{\sim}{U}^{n}_{ijk} - \Delta t\ (\underline{\underline{H}}^{n}_{ijk}\underline{S}_{i+\frac{1}{2}} + \underline{\underline{H}}^{n}_{i-1jk}\underline{S}_{i-\frac{1}{2}}) \qquad (13a)$$

$$\underset{\sim}{U}^{n+1}_{ijk} = \tfrac{1}{2}(\underset{\sim}{U}^{n}_{ijk} + \overline{\underset{\sim}{U}^{n+1}_{ijk}} - \Delta t(\overline{\underline{\underline{H}}^{n+1}_{ijk}}\underline{S}_{i+\frac{1}{2}} + \overline{\underline{\underline{H}}^{n+1}_{i-1jk}}\underline{S}_{i-\frac{1}{2}}$$

$$+ \underline{\underline{H}}^{n}_{ijk}\underline{S}_{i+\frac{1}{2}} + 2\underline{\underline{H}}^{n}_{i-1jk}\underline{S}_{i-\frac{1}{2}} + \underline{\underline{H}}^{n}_{i-2jk}\underline{S}_{i+\frac{1}{2}})) \qquad (13b)$$

where, as before, $\underset{\sim}{U}_{ijk} = \text{vol}_{ijk}\ \underline{U}_{ijk}$.

The operators (8) and (13) were used to obtain the numerical results to be discussed later. Several points are worthy of note. The operator $L_1(\Delta t)$ is applied along rows of the mesh, $L_2(\Delta t)$ along columns and $L_3(\Delta t)$ circumferentially, essentially in a sweep from a left-hand boundary to a right-hand boundary. Focussing on the predictor step (13a), we see that at any interior cell located at i = I, the first flux term appearing on the right-hand side is stored with a reversal of sign for computations at the next cell located at i = I + 1. The fact that some computing is thereby avoided is incidental, the point to be emphasised being that this is a numerical statement of the conservation principle. Continuing on this theme, we observe that when switching within a split between operators (8) and (13), we require transition operators, applied at the switch points, to ensure that strict conservation form is maintained. These operators are best derived in finite volume form, by writing down the two schemes to be connected, at points either side of a switch-point located at i = IS. The necessary flux terms to maintain telescopic cancellation of fluxes through the switch-point can thereby readily be identified. A detailed description of the derivation and resulting transition operators has been given in Ref 15, and will not be repeated here. We end this section with a brief outline of the switching criteria and smoothing terms used in our method.

Switching Criteria and Smoothing Terms

A simple switching criterion which works well on a flow-conforming (H-type) grid is a test on the local Mach number, based upon data at the previous time level. Generally, the best results are obtained with the switch-points located just inside the supersonic region. A typical operator sequence would be

$$L_1^{o/s}(\Delta t)L_2^{m}(\Delta t)L_3^{m}(\Delta t).\underline{U}^{n}_{ijk} \rightarrow \underline{U}^{n+1}_{ijk} \qquad (14)$$

wherein switching occurs in the L_1 split only, the L_2 and L_3 splits being of MacCormack type. Since the upwind operator is stable for time steps twice as large as the MacCormack operator, it is possible that the rate of convergence will be improved if the flowfield is mainly supersonic. However, this will depend upon the magnitudes of the time steps associated with the other splits, which will be dictated by mesh spacings and local flow conditions; the smallest of the three time steps must be used in sequence (14) at any particular cell. For computations on a body-conforming (C-type) grid the switching criterion is generalised, being based on the sign change of the eigenvalue u^{ℓ}-a.

A smoothing term is added to the right-hand side of the corrector step of the MacCormack operator, in the case of the L_1 split only. No added dissipation is required in the case of the upwind operator, or in either of splits L_2 and L_3. Consequently, in problems where the flow is mainly supersonic, with embedded subsonic pockets, very little added dissipation is employed in the algorithm. Shock waves are captured crisply, with no oscillations and without adversely affecting entropy production. The smoothing term is a five-point difference replacement for the derivative $\partial^4 U/\partial x^{\ell 4}$; it is switched on and off conservatively at the switch points as discussed in Ref 15.

Initial Data and Boundary Conditions

The computations were started impulsively by setting the variables in each cell to their respective free stream values. The dependent and derived variables were normalised as follows. Let p, ρ, (w_1,w_2,w_3) and e represent the pressure, density, Cartesian velocity components and total energy per unit volume. Let ρ_∞, $(w_1,w_2,w_3)_\infty$ and L denote the density, velocity components in the freestream and L a typical body dimension. Then

$$\bar{\rho} = \rho/\rho_\infty, (\bar{w}_1,\bar{w}_2,\bar{w}_3), \quad (w_1,w_2,w_3)/(w_1,w_2,w_3)_\infty$$

$$\bar{P} = P/\rho_\infty q_\infty^2,\ \bar{e} = \bar{P}/(\gamma-1) + \bar{\rho}(\bar{w}_1^2+\bar{w}_2^2+\bar{w}_3^2)/2,$$

$$(\bar{X},\bar{Y},\bar{Z}) = (X,Y,Z)/L \text{ and } \bar{t} = \frac{t}{L}\,(w_1,w_2,w_3)_\infty$$

where $q_\infty^2 = (w_1^2+w_2^2+w_3^2)_\infty$ and γ is the ratio of specific heats.

Where a flow conforming grid is used there are four distinct boundary conditions. At the inflow boundary we set the dependent variables to their freestream values. At the outflow boundary, usually a national five body lengths downstream, no boundary condition is required if the exit flow is supersonic. If the exit flow is subsonic, we assume that spatial gradients are negligible. We assume that the far field boundary, placed some ten body-lengths distant, is analogous to a wind-tunnel wall and impose solid wall boundary conditions. We also impose this condition at the configuration surface, where

$$\underline{q}.\underline{g}^{2} = 0 \qquad (15)$$

and derive the required surface static pressure (see Equation (5)) from the normal momentum balance for the cell adjacent to the surface.

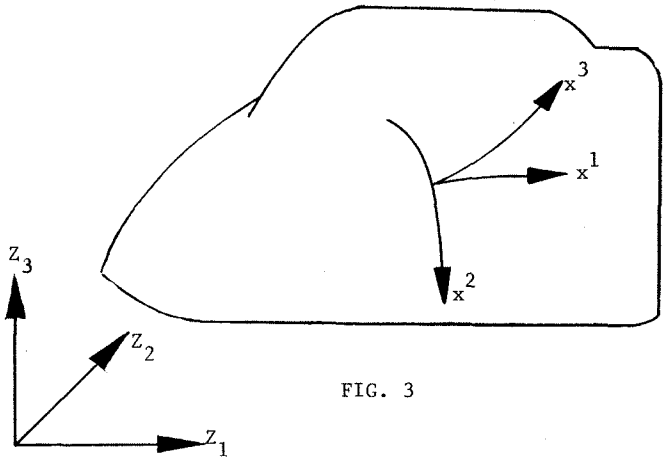

FIG. 3

Taking the inner product between the surface normal vector and the momentum equation we have,

$$g_j^2 \left[\frac{\partial}{\partial t}(\sqrt{g}\rho w_j)+\frac{\partial}{\partial x^\ell}(\rho u^\ell w_j + g_m^\ell a_{mj} p)\right] = 0 \qquad (16)$$

or

$$\frac{\partial}{\partial t}(\sqrt{g}\rho u^2)+\frac{\partial}{\partial x^\ell}(\sqrt{g}\, g_j^2 \rho u^\ell w_j)-\sqrt{g}\,\rho u^\ell w_j \frac{\partial}{\partial x^\ell}(g_j^2)$$
$$+ \sqrt{g}\, g_j^2 g_m^\ell a_{mj} \frac{\partial p}{\partial x^\ell} + g_j^2 p \frac{\partial}{\partial x^\ell}(g_m^\ell a_{mj}) = 0$$

which, when taken with (15), reduces to

$$\sqrt{g}\, g_j^2 g_m^\ell a_{mj} \frac{\partial p}{\partial x^\ell} - \sqrt{g}\,\rho u^\ell w_j \frac{\partial}{\partial x^\ell}(g_j^2) = 0$$

or

$$g_j^2 g_j^\ell \frac{\partial p}{\partial x^\ell} - \rho u^\ell w_j \frac{\partial}{\partial x^\ell} g_j^2 = 0. \qquad (17)$$

Written in finite-volume notation,

$$p_b = p_c - \frac{\Delta x^2}{S_j^2 S_j^2}\left[\rho u^\ell w_j \frac{\partial}{\partial x}(S_j^2) - S_j^2 S_j^3 \frac{\partial p}{\partial x^3} - S_j^2 S_j^1 \frac{\partial p}{\partial x^1}\right] \qquad (18)$$

where p_b is the required surface pressure, p_c is the pressure at the centre of the adjacent cell and $S_j^\ell = \sqrt{g}\, g_j^\ell$; for the same cell.

Results and Discussion

Before we begin a discussion of the axisymmetric and three dimensional flow cases we illustrate the validity of the operator-switching algorithm for the test problem used earlier in Fig. 2. This is the NACA 0012 aerofoil, at Mach 0.85 and $\alpha = 0^o$, with computations performed on a C-type grid. The only changes to the above boundary procedures occur at the farfield boundary where we invoke as many boundary conditions as there are inward pointing characteristics. We also, in lifting cases, model a compressible vortex in the outer ring of cells. Fig. 4 shows the surface C_p and entropy distributions for direct comparison with Fig. 2. A further range of test problems, which demonstrate the method's intrinsic validity, have been computed and reported earlier in Ref.22.

Axisymmetric 'Aircraft Forebody'

Our axisymmetric flow example is a simulated military aircraft fuselage, in which the upper meridian line has been rotated about the aircraft longitudinal axis to generate a body of revolution, see Fig. 5. The nose cone is conical with a half angle of 20^o. Behind the conical section the contour BC is faired out, its slope being zero at C. The section CD, representing the canopy windshield, is also conical with a half angle of 30^o. The remaining portion of the canopy, DE, is defined by a quartic polynomial, smoothly fairing into the semi-infinite afterbody.

The equations defining the body contour are

$$y_{AB} = 0.365x \qquad 0 \leq x \leq 1$$

$$y_{BC} = 0.365\ (x-(x-1)^2/12) \qquad 1 \leq x \leq 7$$

$$y_{CD} = 1.46 + 0.577\ (x-7) \qquad 7 \leq x \leq 8$$

$$y_{DE} = 1.46 + 0.577\ (1.3x-9.4)\ (1.8-0.1x)^3 \qquad 8 \leq x \leq 18.$$

The body is set at zero angle of attack at an incident Mach number of 1.40. We anticipate at least two shock waves will form, one attached to the nose and another standing upstream of the canopy, with a subsonic pocket around the windshield. In the recompression zone behind the canopy, characteristics leaving the body surface may coalesce in the field to form an embedded shock wave. The numerical results were obtained by using a two-dimensional form of the method, with an appropriate correction applied to the difference operators to reflect the axial-symmetry of the flow. In this context, it is worthy of note that the solutions are not adversely affected by the singularity on the axis, since the method is cell-centre orientated, rather than node-point orientated.

We begin with a direct comparison between the MacCormack and Operator-switching methods. Naturally we have available distributions of all dependent variables and certain derived quantities, namely, static pressure, entropy and total pressure. Some, however, are notably more sensitive to perturbations in the solution methodology (including the mesh) than others, and here we focus respectively on the Mach number and entropy distribution , the latter quantity being particularly sensitive. Fig. 6 shows the axial Mach number distribution in the body surface row of cells. We see that the bow shock is attached and that the canopy shock is detached, followed by a substantial subsonic pocket. It is clear that the operator-switching (O/S) algorithm everywhere yields a smoother, less oscillatory, solution compared with the MacCormack algorithm. Discrepancies are uncompromisingly laid bare in Fig. 7, depicting the respective entropy distributions. The O/S distribution is evidently less noisy and the expected step rises more clearly defined. However, in the region of the canopy windshield (x=8), where the flow is

expanding very rapidly, the O/S result is rather noisy. By changing slightly the local mesh refinement, as shown in Fig. 8, this behaviour can be erradicated.

Figure 9 depicts the convergence histories of the two algorithms, based on a field r.m.s. residual. Of particular note is the fact that both algorithms converge rapidly following the rigours of the impulsive start. We observe that a 'softer' starting procedure may therefore yield tangible benefits, particularly in relation to entropy spikes and spurious entropy production. Also, not immediately obvious is the fact that, for both algorithms, the $L_2(\Delta t)$ operator is driving the solution in each cell. Because this operator is, in both cases, of MacCormack type the weaker stability bound of the upwind scheme is not capitalised upon. It is possible that by increasing the transverse mesh interval, adjacent to the body, the $L_1(\Delta t)$ operator will drive the solution and the rate of convergence will be increased, but this may not be compatible with the required spatial resolution. Further discussion of the interconnected role of mesh spacings, splittings and associated time steps may be found in Ref.23. Here we merely observe that by implementing, as a refinement of the method, local operator sequences as suggested in Ref. 15 convergence may be improved a little. However, the rate of convergence observed in the present case in anyway high, the computations requiring approximately 45 seconds on a CDC 7600 computer.

Fig. 10 shows the effect of mesh shearing and grading. Once again the entropy distributions (Fig. 10c) show the differences most clearly. Here the entropy rise behind the shock has been halved by aligning the transverse coordinate lines approximately with the bow shock. Although the differences here are particularly marked we note that in terms of Mach number they are less obvious and differences in C_p (not shown) are hardly discernible. No attempt was made to achieve alignment with the canopy shock, the resolution of which accordingly is not improved. By implementing a simplified form of adaptive grid software locally in the near field it appears likely that highly accurate solutions will obtain. Further, Fig. 11 shows the effect of changing the amount of smoothing applied to the $L_1(\Delta t)$ operator. This further reduces, by approximately 40% the entropy level behind the bow shock. This, when combined with shearing of the mesh yields an entropy rise close to the exact level expected behind the conical bow shock.

Finally Figs. 12, 13 depict the body surface C_p distribution and field isobar contours for later comparison with the three dimensional results.

Three-Dimensional Aircraft Forebodies

We begin by presenting some results which illustrate the validity of the three dimensional method. All of the meshes employed in this section are, essentially, of cylindrical polar, flow conforming type and relatively coarse. Remarks concerning improvements to the mesh generation process, in the light of future applications of this method, are deferred to the next section. An application of the three-dimensional code to the axisymmetric forebody of the previous section, at the same Mach number and zero angle of attack, would be expected to yield comparable results to those already presented. Figs. 14, 15 show, respectively the axial C_p distribution along the body surface row of cells, and an isometric view of the surface isobar contours. As expected, the contours are θ invariant and the C_p distribution is comparable to that shown earlier in Fig. 12.

A further example, for which experimental data is available, relates to Forebody No. 4, taken from Ref. 24, from which an analytical definition of the body geometry can be found. The chosen Mach number is 1.70 and the angle of attack is -5^o. At zero angle of attack the flow over the body is everywhere supersonic and the problem is amenable to solution by space marching. However at $\alpha=-5^o$, the flow in the marching direction becomes subsonic and space marching is no longer possible[25], therefore time-marching must be employed. Fig. 16a provides a comparison with data of axial C_p distributions on the body surface as a function of the circumferential angle θ, summarised in the isobar contours of Fig. 16b. In view of the relative coarseness of the mesh employed in the computations (60 x 10 x 8) the agreement is satisfactory.

We now move to more realistic three-dimensional forebody simulations. Two simulations will be discussed. The first, shown in Fig. 17, is a three-dimensional version of the earlier axisymmetric forebody, in which the canopy is faired-out through a surface discontinuity in the θ direction. The body, so constructed, is a realistic hypothetical model of a fighter aircraft forebody. The canopy shock is therefore expected to vanish in axial distributions over the lower half of the body. Isometric surface isobar plots, as shown in Fig. 17b, are supplemented in practice by field contours, Fig. 17c, and cross-flow contour maps (not shown). In this case the incident Mach number is 1.40 and the angle of attack is 0^o.

Finally, the second example relates to a more complex forebody, having a (5^o) dipped elliptical (rather than conical) nose cone and relatively flat sides and underside to accommodate canard foreplanes, and side or chin intakes in a later study. Here the incident Mach number is 1.40 and the angle of attack is -5^o. Fig 18 depicts the forebody contour and computed surface isobar contours. The computations were performed on a relatively coarse mesh (57 x 10 x 18) and tests are underway to obtain further numerical results as the mesh is refined. The three-dimensional examples shown required approximately 480 seconds on a CDC7600 computer.

Mesh Generation

There is clearly scope for refinement of the simple mesh generation procedure which we have used to obtain the three-dimensional results. Probably the biggest deficiency in our meshes is the rate at which cells grow in size as one moves into the farfield, particularly if exponential stretching is employed as it is here. An improved procedure has been presented recently by Arlinger[26]. A typical mesh, generated for a

section through an aircraft forebody, is shown in Fig. 19 and compared with the cylindrical polar variety.

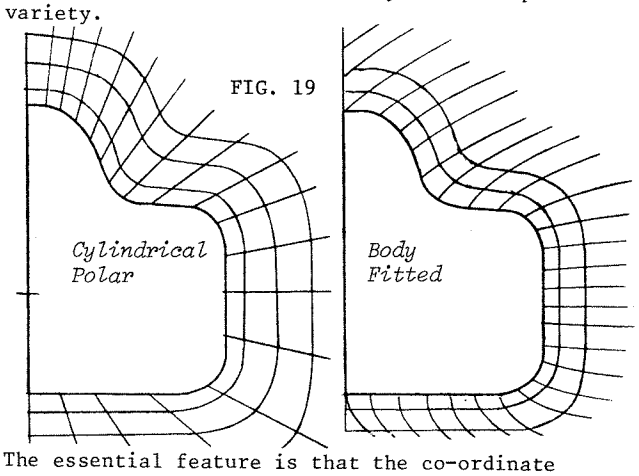

FIG. 19

The essential feature is that the co-ordinate lines are body-fitted in the near-field and 'relax' into the Cartesian frame in the far-field.

An important constraint which any chosen procedure should satisfy is that it be readily extendable to treat more complete aircraft configurations. The Arlinger procedure would imply the use of an H-type mesh around the wing, or alternatively, a mesh-patching arrangement wherein a C-type patch is placed around the leading-edge of the wing.

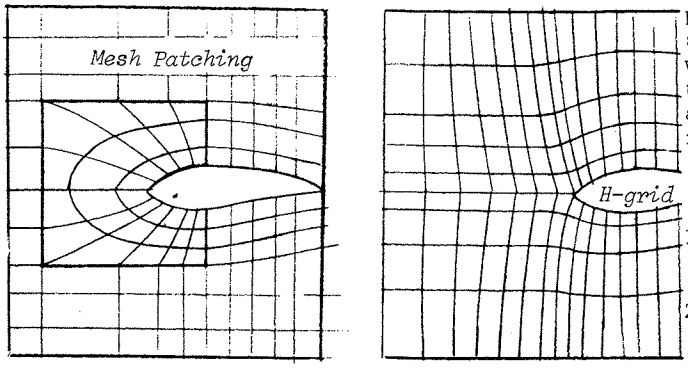

The difficulty with the C-C and O-O type meshes currently widely employed for the study of isolated wings and wing-fuselage interactions is the inadequate resolution of the forebody.

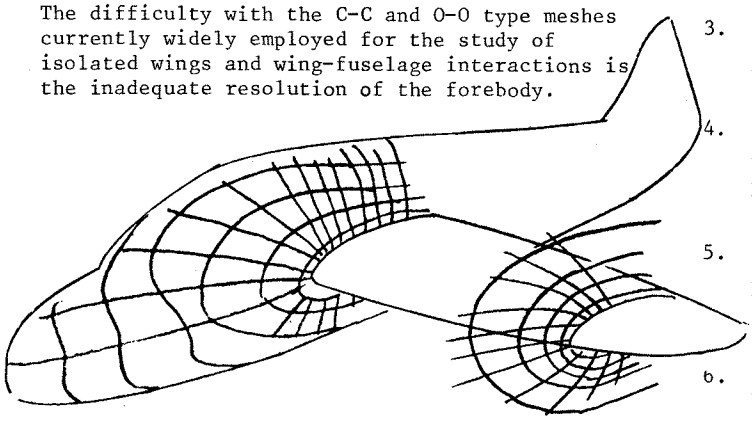

It seems likely, therefore, that some form of mesh patching will be required if H-type treatments of the wing are unsatisfactory. The extensive research activity in this area may in the near future clarify the most appropriate procedure. Ref. 27 is a recent review.

Concluding Remarks

A computational method has been presented for time-marching solutions of the Euler equations around realistic aircraft forebodies in transonic flow. The method is versatile, robust and has good shock capturing capabilities. We have compared the presented Operator-Switching method with that of MacCormack, commenting on the inter-connected role of time steps, mesh spacings and splittings, and remarked on anticipated refinements to our simple mesh generation procedure for future applications to more complete aircraft configurations.

As was observed in the introduction to this paper, there is a sense in which the available methods can be viewed in a heirarchal light, in the sense of increasing accuracy in the model, algorithm complexity and computing cost. The relatively inexpensive potential methods can produce useful data for quite complex configurations for use in preliminary design, having in mind their intrinsic limitations. Whilst the expensive flux-splitting methods can be used for the accurate resolution of very strong shock-waves, or for calibrating other Euler methods. Since they have yet to be applied to the complex three-dimensional geometries found in the aeronautical field, there may be some juxtaposition for superiority amongst Euler solvers. However, in practice, the designer will choose the method most suitable for a given problem. Sometimes a potential method will be sufficient, other times a flux-splitting method will be required. We believe Euler solvers of the type described here can offer the most viable alternative for most aeronautical problems requiring an inviscid solution.

References

1. Magnus, B and Yoshihara, H. Inviscid Transonic Flow Over Airfoil, JAIAA, Vol. 8, No. 12, 1970

2. Murman, E.M. and Cole, J.D. Calculation of Plane Steady Transonic Flows, JAIAA, Vol. 9. No. 1, 1971.

3. Reyhner, T.A. Transonic Potential Flow Computation About Three Dimensional Inlets, Ducts and Bodies, AIAA Paper No. 80-1364,1980

4. Boppe, C.W. Computational Transonic Flow About Realistic Aircraft Configurations, AIAA Paper, No. 78 -104, 16th Aerospace Sci. Mtg., 1978.

5. Salas, M.D., Jameson, A. and Melnik, R.E. A Comparative Study of the Non-Uniqueness Problem of the Potential Equation, AIAA Paper, No. 83-1888, 6th CFD Conf., 1983.

6. Lerat, A. and Sides, J. A New Finite Volume Method for the Euler Equations with Application to Transonic Flows, Num. Meths. Aero. Fluid Dyn., P.L. Roe (Ed.), Academic Press, 1982.

7. Jameson, A., Schmidt, W. and Turkel, E. A Numerical Solution of the Euler Equations by Finite-Volume Methods Using Runge-Kutta Time Stepping Schemes, AIAA Paper No. 81-1259, 1981.

8. Denton, J.D. An Improved Time-Marching Method for Turbomachinery Flows, Num. Meth. Aero. Fluid Dyn., P.L. Roe (Ed.), Academic Press, 1982.

9. Rizzi, A. A Damped Euler Equation Method to Compute Transonic Flow Around Wing-Body Combinations, JAIAA, Vol. 20, 1982.

10. Roe, P.L. Approximate Riemann Solvers, Parameter Vectors and Difference Schemes, J. Comp. Phys., Vol. 43, p 321-352, 1981.

11. Roe, P.L. Numerical Modelling of Shock Waves and other Discontinuities, Num., Meth., Aero., Fluid Dyn., P.L. Roe (Ed.) Academic Press,1982

12. Osher, S. Shock Modelling in Aeronautics Num. Meths. for Fluid Dyn., K.W. Morton and M.J. Baines (Ed.), Academic Press, 1983.

13. Yang, J.Y., Lombard, C.K. and Bershader, D. A Characteristic Flux-Difference Splitting for the Hyperbolic Conservation Laws of Inviscid Gas Dynamics, AIAA Paper No. 83-0040, 1983.

14. Chakravarthy, S. Numerical Experiments with the Osher Upwind Scheme for the Euler Equations, AIAA Paper No. 82-0975, 1982.

15. Causon, D.M. and Ford, P.J. Improvements in Techniques for the Numerical Simulation of Steady Transonic Flows, AIAA Paper No. 84-0089, 22nd Aerospace Sci. Mtg., 1984.

16. Kordulla, W., and Vinokur, M. Efficient Computation of Volumes in Flow Predictions, JAIAA, Vol 21, 1983.

17. Strang, G. On the Construction and Comparison of Difference Schemes. SIAM J.of Num. Anal., Vol. 5, p 506-517, 1968.

18. Harten, A., and Zwas, G. Self-Adjusting Hybrid Schemes for Shock Computations, J. Comp. Phys., Vol. 9, p 568, 1972.

19. Jameson, A. Steady-State Solution of the Euler Equations for Transonic Flow, Adv. in Sci. Comp., Transonic Shock and Multi-dimensional Flows, Meyer R E(Ed.),Academic Press, 82.

20. Rizzi, A. Computations in Rotational Transonic Flow, Num. Meth. for the Comp. of Inv. Transonic Flow, A GAMM Workshop, Rizzi, A. and Viviand, H. (Ed.) Vieweg, 1981.

21. Warming, R.F. and Beam, R.M. Upwind Second-Order Difference Schemes and Applications in Aerodynamic Flows, JAIAA Vol. 14, 1976.

22. Causon, D.M. and Ford, P.J. Computations in External Transonic Flow, 5th GAMM Conf. on Num. Meth. in Fl. Mech., Vieweg, 1984.

23. Causon, D.M. and Ford, P.J. The Calculation of Axisymmetric Flows Over Bodies at High Speeds, Internal Report CAG No. 8410, Dept Aero and Mech Eng., Univ. of Salford, UK,1983.

24. Townsend, J.C., Howell, D.T., Collins, I.K. and Hayes, C. Surface Data on a Series of Analytic Forebodies at Mach Numbers from 1.70 to 4.50 and Combined Angles of Attack and Sideslip. NASA TM-80062, 1979.

25. Shankar, V., Szema, K.Y. and Osher, S. A Conservative Type-Dependent Full-Potential Method for the Treatment of Supersonic Flows with Embedded Subsonic Regions, AIAA Paper No. 83-1887, 6th CFU Conf. 1983.

26. Arlinger, B. Computation of Supersonic Flow Around Bodies, AIAA Paper No 84-0259, 22nd Aerospace Sci Mtg., 1984.

27 Numerical Grid Generation Techniques Proc. of Workshop sponsored by NASA and the Inst. for Computer Applic. in Sci. and Eng., held at NASA Langley Research Centre, 1980, NASA CP-2166.

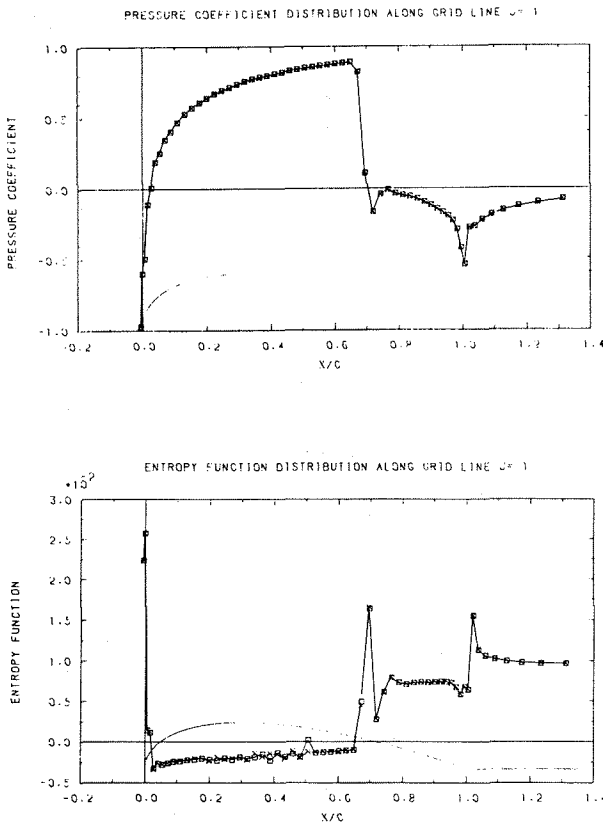

FIG. 4 NACA 0012 AEROFOIL AT M = 0.85 AND $\alpha = 0^{o}$

$$entropy\ function = (p/\rho^{\gamma})/(p/\rho^{\gamma})_{\infty}$$

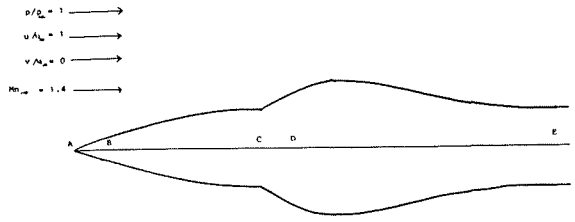

FIG. 5a BODY CONTOUR

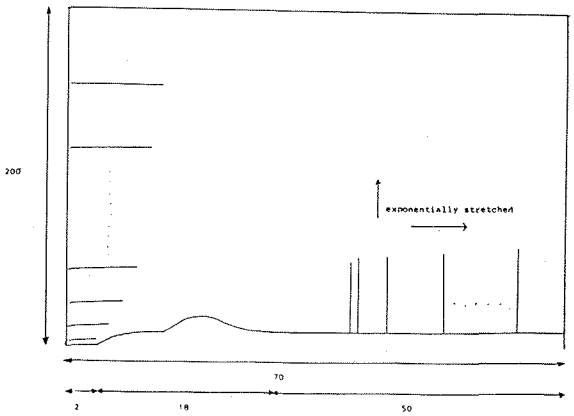

FIG 5b COMPUTATIONAL DOMAIN

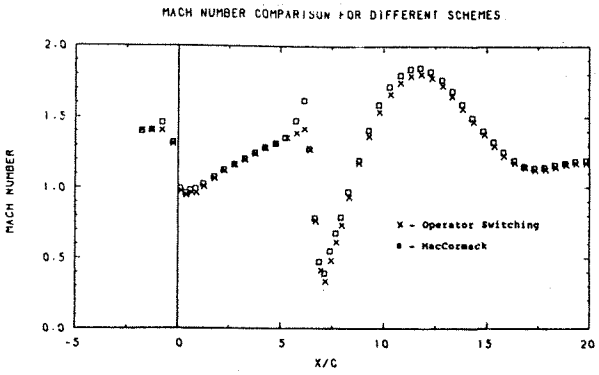

FIG. 6

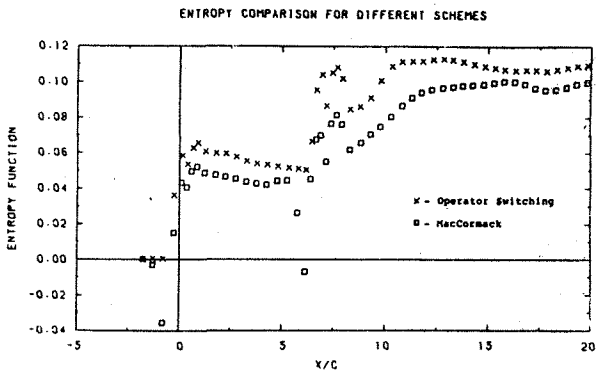

FIG. 7

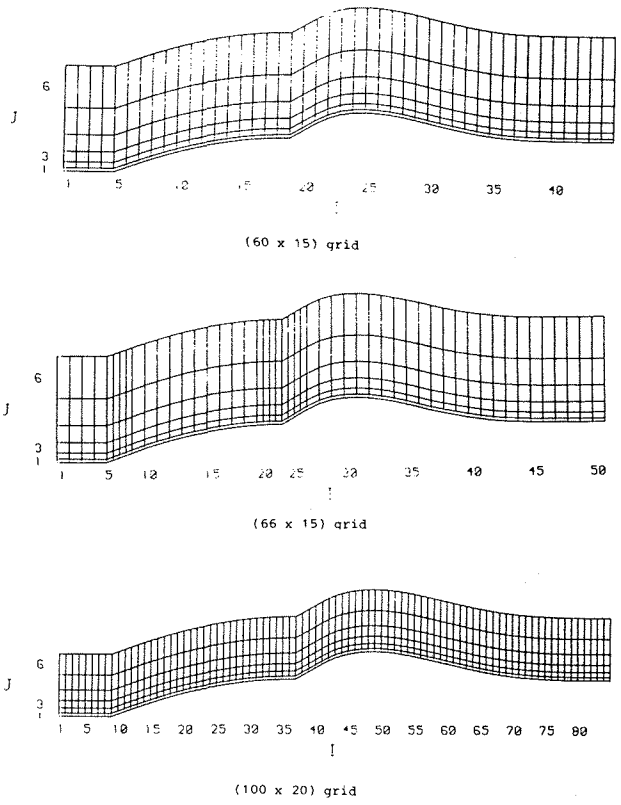

FIG. 8a MESH REFINEMENT

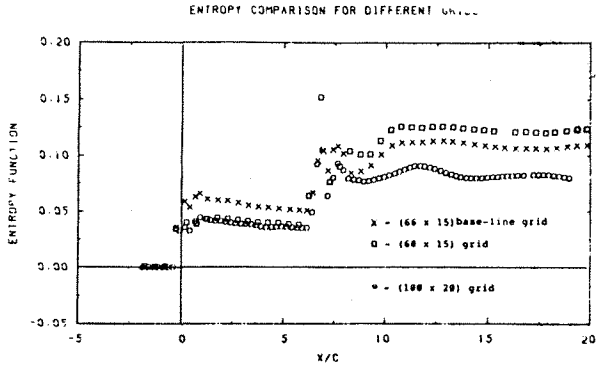

FIG. 8b

AXISYMMETRIC 'AIRCRAFT FOREBODY' AT MACH 1.40 AND ALPHA = 0°

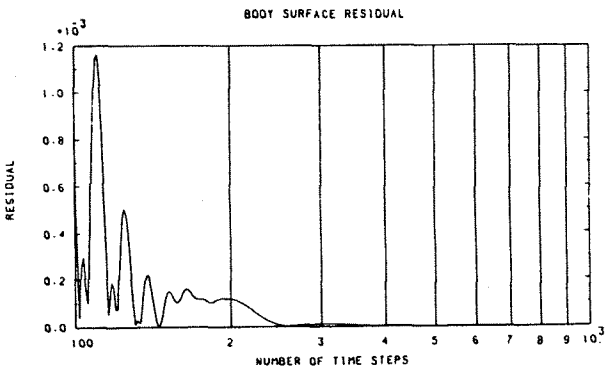

FIG. 9a MacCormack

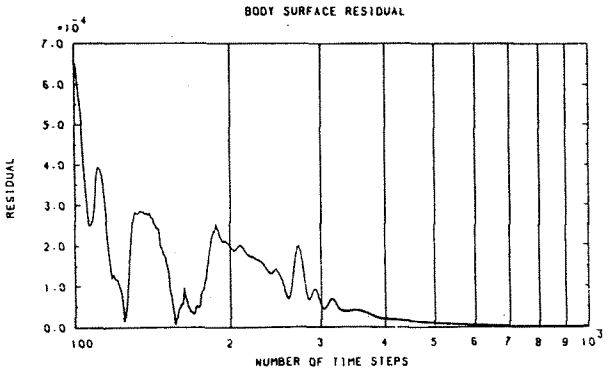

FIG. 9b Operator-Switching

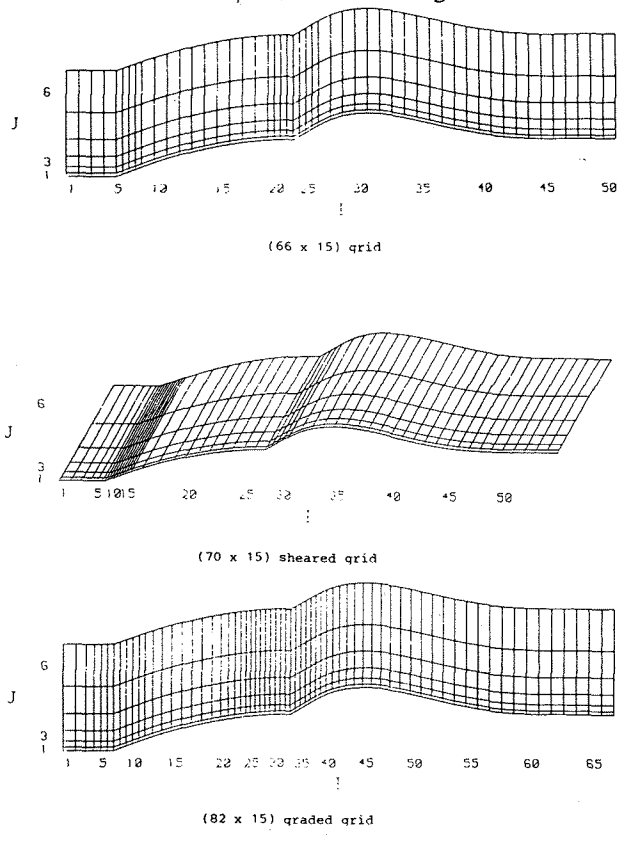

FIG. 10a MESH SHEARING AND GRADING

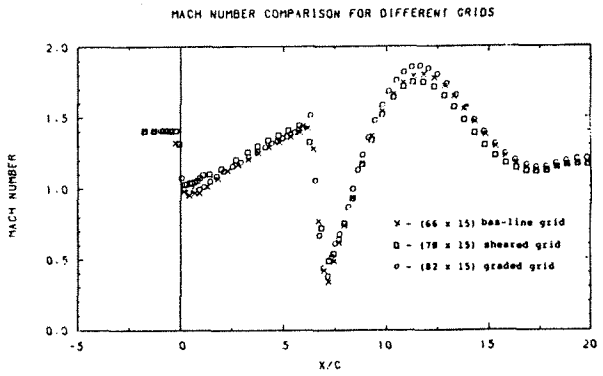

FIG. 10b

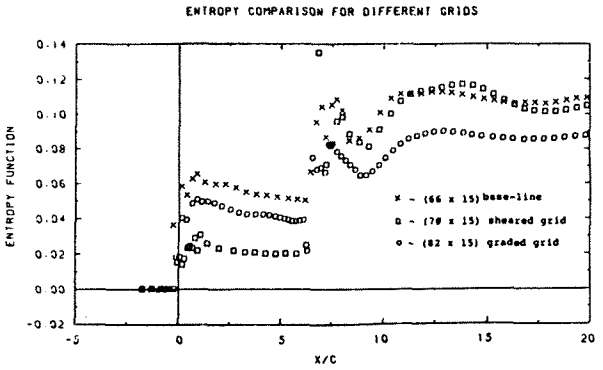

FIG. 10c

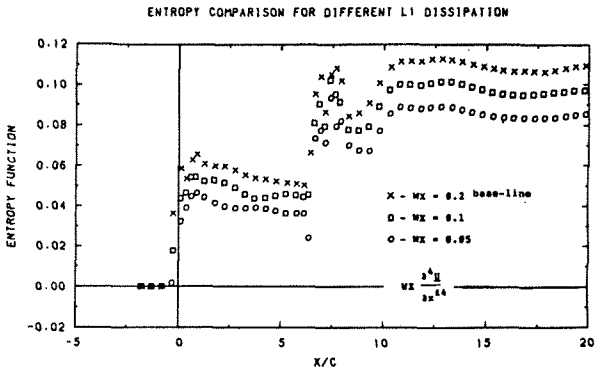

FIG. 11

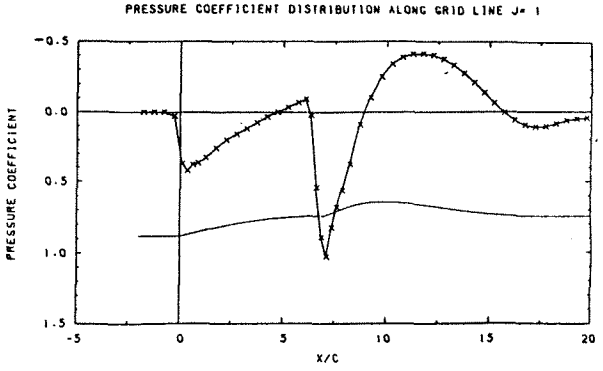

FIG. 12

AXISYMMETRIC 'AIRCRAFT FOREBODY AT MACH 1.40 AND ALPHA = 0^{o}

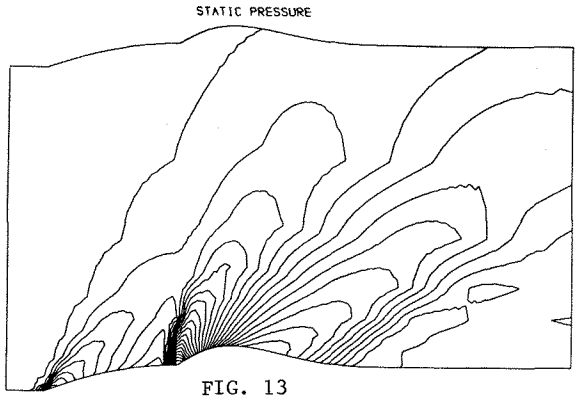

FIG. 13

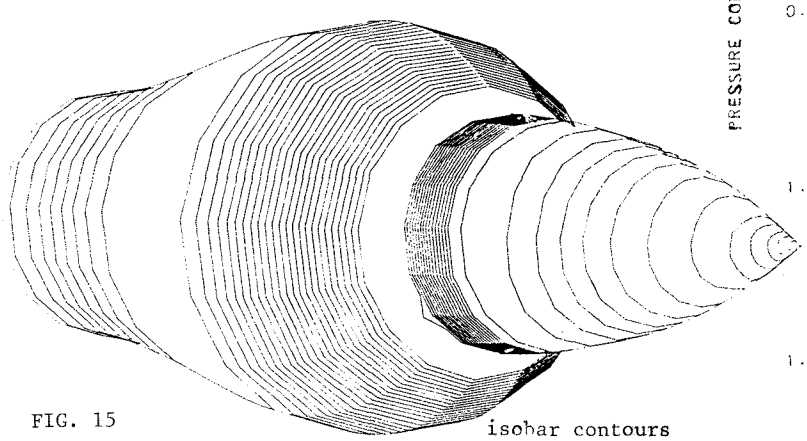

FIG. 15 isobar contours

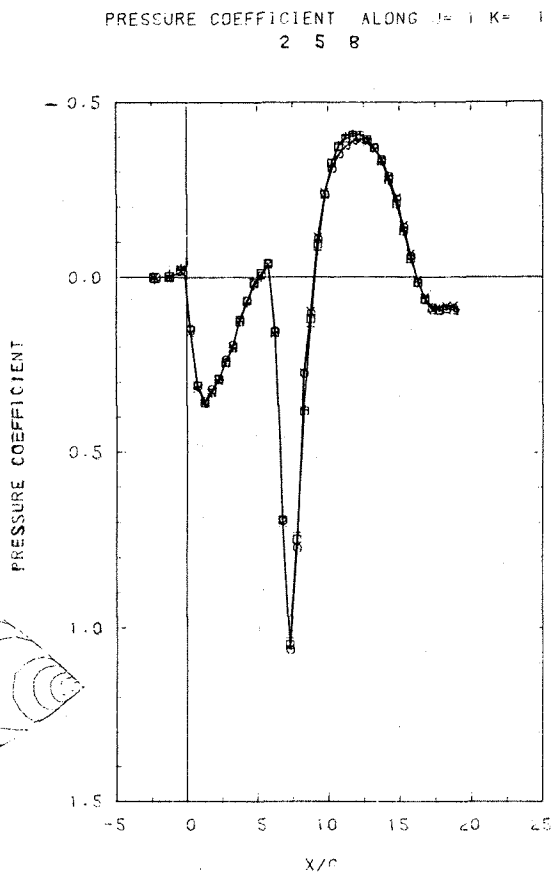

FIG. 14

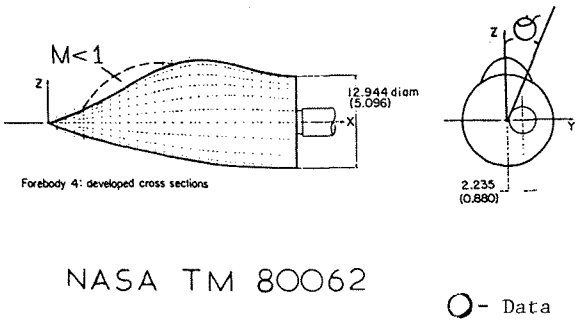

NASA TM 80062

O- Data

NASA TM80062 Forebody No 4 Mach 1.70, α = -5°

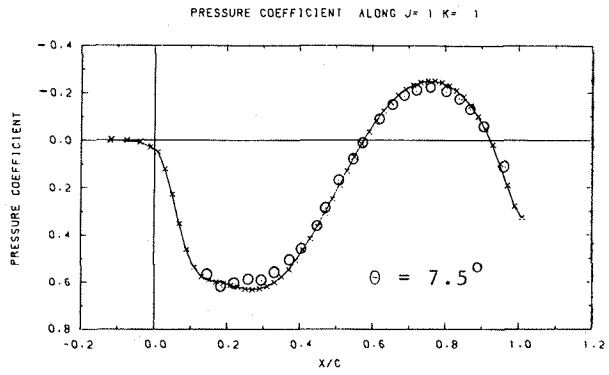

FIG. 16a

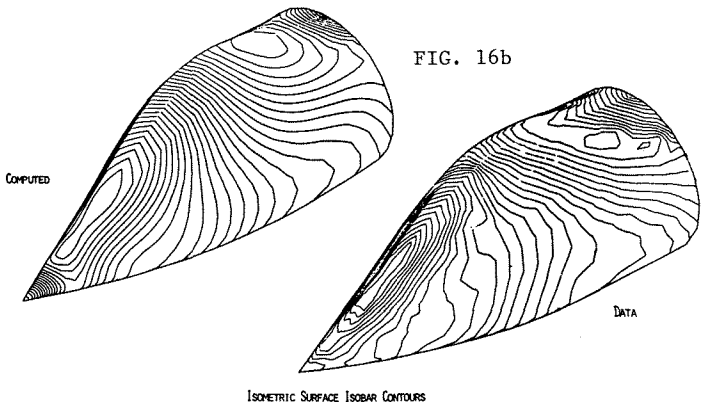

FIG. 16b

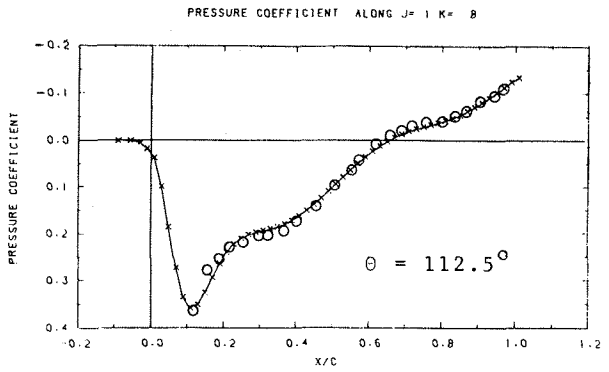

FOREBODY NO 4 FROM NASA TM80062 AT MACH 1.70 AND ALPHA = - 5° IN ZERO-SIDESLIP CONDITION

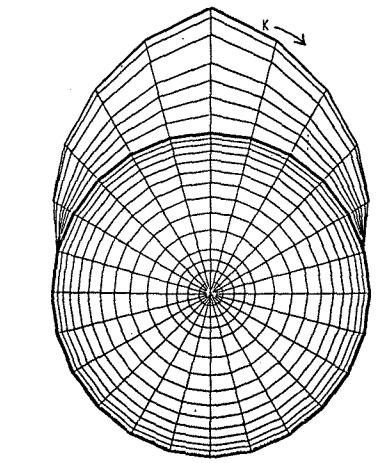

HYPOTHETICAL AIRCRAFT FOREBODY - FRONT ELEVATION

FIG. 17

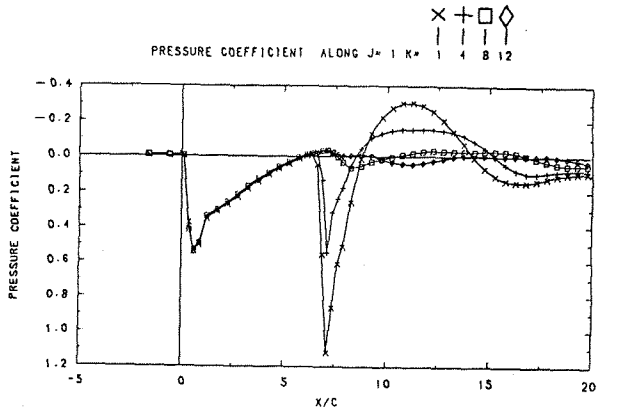

HYPOTHETICAL AIRCRAFT FOREBODY AT MACH 1.40, $\alpha = 0^{\circ}$ IN ZERO-SIDESLIP CONDITION

(a)

(b)

ISOMETRIC SURFACE ISOBAR CONTOURS - STARBOARD SIDE

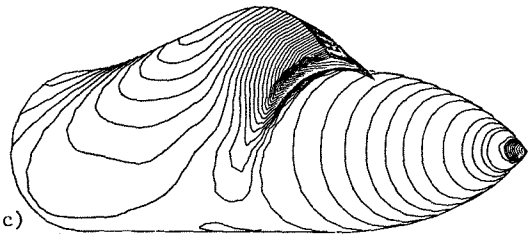

(c)

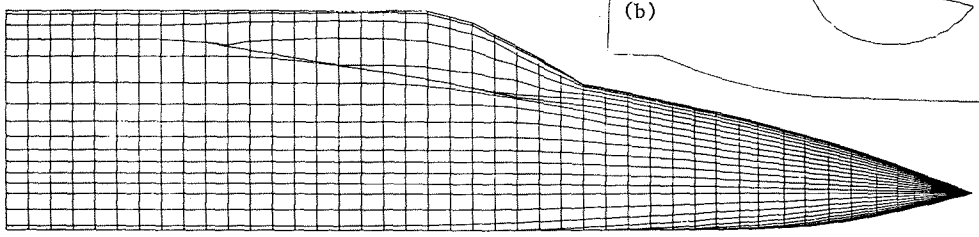

(a)

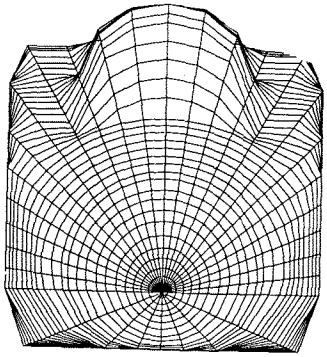

(b)

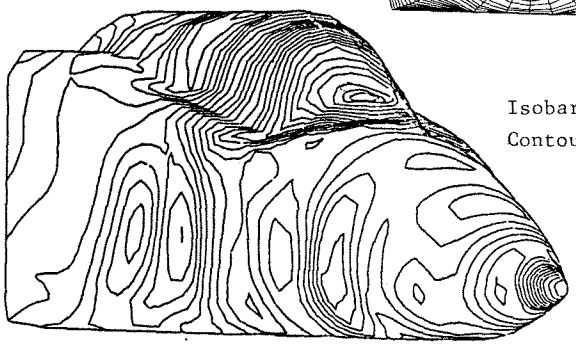

Isobar Contours

(c)

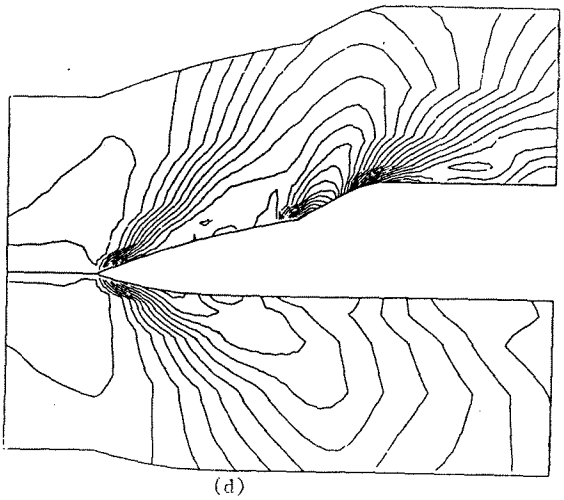

(d)

FIG. 18 SIMULATED REALISTIC AIRCRAFT FOREBODY AT MACH 1.40 AND ALPHA = - 5° ZERO-SIDESLIP CONDITION